SCIENTIFIC REPORTS

OPEN

SUBJECT AREAS:
METASTASES
CELL BIOLOGY
UROLOGICAL ONCOLOGY

Received
12 August 2013

Accepted
18 October 2013

Published
6 November 2013

Correspondence and requests for materials should be addressed to D.R.B. (diane.bielenberg@childrens.harvard.edu) or B.R.Z. (bruce.zetter@childrens.harvard.edu)

* Current address: UM Cancer Research Institute, Department of Pharmacology, Faculty of Medicine, University of Malaya, 50603 Kuala Lumpur, Malaysia.

† Current address: Prestizia, 9, Avenue de l'Europe, F-34830 Clapiers, France.

‡ Current address: Institut Régional contre le Cancer, 3, rue de la Porte de l'Hôpital 67085 Strasbourg cedex.

Regulation of epithelial plasticity by miR-424 and miR-200 in a new prostate cancer metastasis model

Jacqueline Banyard[1,2], Ivy Chung[1,2]*, Arianne M. Wilson[1], Guillaume Vetter[3]†, Antony Le Béchec[3]‡, Diane R. Bielenberg[1,2] & Bruce R. Zetter[1,2]

[1]Vascular Biology Program, Boston Children's Hospital, Karp Family Research Laboratories, 300 Longwood Ave., Boston, MA 02115, [2]Department of Surgery, Harvard Medical School, Boston, MA 02115, [3]Cytoskeleton and Cell Plasticity lab, Life Sciences Research Unit-FSCT, University of Luxembourg, L-1511 Luxembourg, Luxembourg.

Using an *in vivo* cycling strategy, we selected metastatic cancer cells from the lymph nodes (LN) of mice bearing orthotopic DU145 human prostate tumors. Repeated rounds of metastatic selection (LN1–LN4) progressively increased the epithelial phenotype, resulting in a new model of tumor cell mesenchymal-epithelial transition (MET). DU145-LN4 showed increased cell-cell adhesions, higher expression of multiple epithelial markers, such as E-cadherin, EpCAM and cytokeratin 18, and reduced expression of mesenchymal markers such as vimentin. The MET in DU145-LN4 cells was accompanied by increased expression of the miR-200 family, and antimiRs to miR-200c and miR-141 induced an EMT. MET also correlated with the loss of miR-424. Ectopic transient and stable miR-424 expression induced EMT, with reduced epithelial marker expression and increased cell scattering. Our model provides evidence for spontaneous MET *in vivo*. We show that this cellular plasticity can be mediated through the combined action of miR-424 and the miR-200 family.

Metastases are responsible for most cancer deaths[1]. Metastasis is a complex, multistep process that still remains poorly understood. Cells must first escape from the primary tumor mass, invade surrounding extracellular matrix, intravasate into lymphatic and blood vessels and establish secondary tumors. Initial steps in this process are aided by the phenotype and gene expression changes that occur during epithelial-mesenchymal transition (EMT). During tumor cell EMT, cell-cell junctions are lost and cells become more motile, secrete proteases and re-express many markers in the embryonic EMT differentiation program[2]. These characteristics promote invasion and dissociation. However, there is controversy surrounding the role of EMT in metastasis *in vivo*[3–6]. Pathology studies indicate that metastases usually show a similar heterogeneous epithelial architecture to the primary tumor[7], despite suggestions that stem-like disseminating tumor cells are responsible for metastasis formation during early stages of primary cancer growth[8]. As metastases display a dominantly epithelial phenotype, it would follow that tumor cells show plasticity, undergoing the reverse process, a mesenchymal to epithelial transition (MET) in order to grow and successfully establish a nodule at the metastatic site[9]. Despite a massive literature supporting the role of EMT in cancer, there has been limited evidence for MET. Several key studies provided evidence for an MET *in vivo*[10–12], and two recent studies have provided convincing evidence of the requirement for MET in metastasis formation. Tsai *et al.* showed that a Twist-induced EMT must be reversed in order for squamous cell carcinoma metastases to form[13], and Ocaña *et al.* showed that suppression of the EMT-inducing homeobox factor, Prrx1, was required for the formation of breast cancer metastases[14].

Cellular plasticity may be influenced by many factors including other tumor cells, cells in the microenvironment, or extracellular matrix[15]. MicroRNAs (miRNAs) have also been established as key regulators of EMT[16,17], and many down-regulate well established EMT-associated transcription factors, such as ZEB1, ZEB2, TWIST, Oct-4 and SNAI1. The relative importance of various miRNA species in tumor plasticity and the crosstalk between them is not yet understood.

Prostate cancer is the second leading cause of cancer-related death for men in the US, with most of the estimated 28,000 yearly deaths resulting from metastases[18]. Predictive models in prostate cancer show that lymph node metastasis results in a poorer prognosis for patients, compared to patients without lymph node involvement[19,20]. Tumor cell escape via lymphatic vessels to the sentinel lymph node may represent a stepping stone for more widespread metastasis via the vascular system to distant organs, such as bone[21]. Understanding the

mechanisms of lymph node metastasis could facilitate the development of new biomarkers and therapeutic options. This may be especially important in prostate cancer as more patients opt for a 'watchful waiting' or active surveillance strategy to manage organ-confined disease[22].

In this report we have used an orthotopic mouse model of prostate cancer metastasis, and have repeatedly selected spontaneous metastases from the sentinel lymph nodes. Human cancer cell xenografts in the orthotopic site are provided relevant environmental signals compared to an ectopic (often subcutaneous) site, resulting in enhanced tumorigenicity[23]. The microenvironment is well established to influence tumor cell behavior, capable of stimulating or repressing cell plasticity, proliferation, migration and invasion[24–26]. The selection of highly metastatic variants from regional lymph node metastasis following orthotopic prostate xenografts has been reported using PC-3 and LNCaP prostate cancer cells[23,27]. These cells have proven highly valuable to the prostate cancer research community. In this report we describe a new model developed using the DU145 human prostate cancer cell line. DU145 is a widely used "classical" prostate cancer cell line that was originally isolated from a brain metastasis[28]. We show that the DU145 metastatic cell variants have undergone a MET which is mediated via the combined action of multiple miRNA species.

Results

Development of a new prostate cancer metastasis model. To select for prostate cancer cells with increased metastatic potential we used an *in vivo* cycling strategy[23,27] to establish a series of sublines from the DU145 human prostate cancer cell line[28]. To establish this model, 2×10^6 DU145 cells were injected orthotopically into the prostate of nude mice. Tumor growth was monitored by abdominal palpation. Once the tumor was 0.5–1 cm in diameter (5–12 weeks), the mice were euthanized and necropsied in a sterile environment. The sentinel paraaortic lymph nodes were excised, minced and the cells were placed into culture (schematic in Figure 1A), as described in Methods. Primary lymph node cultures contained tumor cells and fibroblasts, but after several passages only tumor cells remained and were named DU145-LN1. Repeated rounds of lymph node excision and tumor cell reinjection were performed to establish the DU145-LN2, DU145-LN3 and DU145-LN4 cell lines. RT-PCR was used to confirm that the cell cultures were not contaminated with cells of mouse origin (e.g. fibroblasts) which might affect tumor growth (Supplementary Figure 1A).

To validate our metastasis model, all of the newly established cell lines were injected orthotopically into the prostate of mice at the same time point in a head-to-head comparison. Tumors and lymph nodes were removed after 5 weeks (Figure 1B). Tissues were fixed in formalin and embedded in paraffin for immunohistochemical analysis. Tumor incidence was 100% for all cell lines, while tumor size increased dramatically in cycled lines (Table 1). Lymph node sections (3 tissue levels per node, 4–6 mice per group) were analyzed by H&E staining and human cytokeratin-18 (K18) staining. Lymph node metastasis was measured as incidence of cytokeratin-18 positive tumor foci (single K18+ cells were excluded). Metastatic

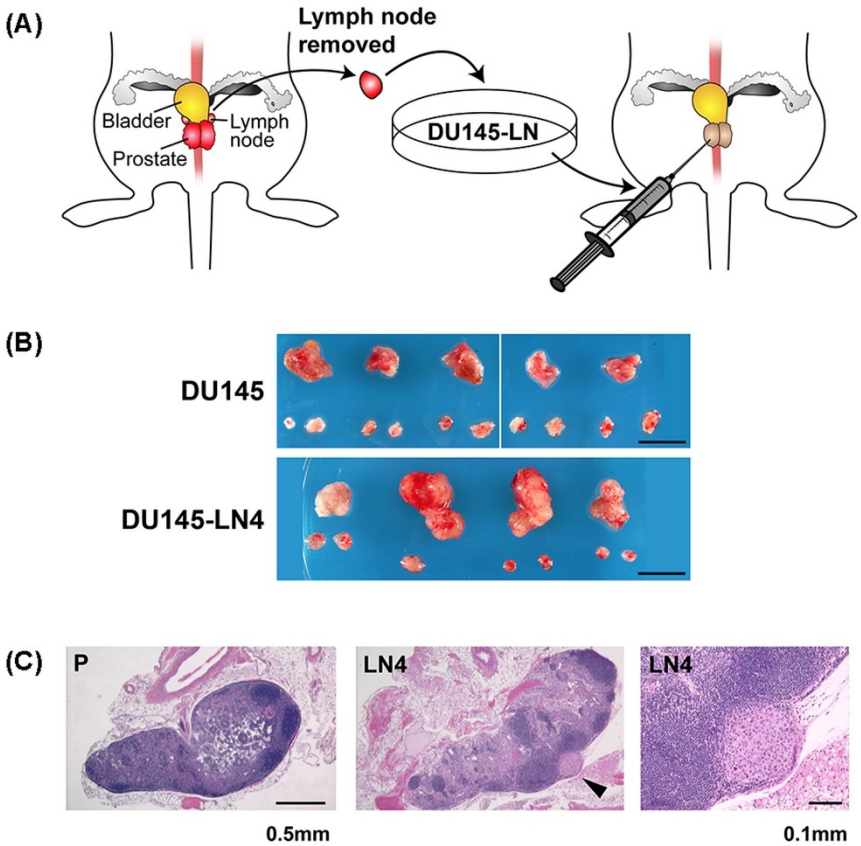

Figure 1 | Selection of DU145 human prostate cancer cells with increased metastatic potential. (A) Schematic of the experimental approach. DU145 prostate cells were injected orthotopically into the prostate. Lymph nodes were removed and cultured, and selected tumor cells subjected to repeated rounds of orthotopic injection. Illustrations by Kristin Johnson (Vascular Biology Program, Boston Children's Hospital). (B) Photography of gross specimens (tumors and sentinel lymph nodes). DU145 parental cells and DU145-LN sublines (DU145-LN4 shown) were reinjected into the prostate and the prostate and lymph nodes were removed after 5 wks. Scale bar = 1 cm. (C) Representative H&E staining of lymph nodes from mice bearing orthotopic parental DU145 tumors (left panel, P) and DU145-LN4 tumors (center and right panels, LN4). Metastatic nodule indicated by arrowhead in center panel, magnification shown in right panel.

Table 1 | *In vivo* growth of DU145 sublines

Cell Line Injected	Tumor Incidence	Mean Tumor Volume ($mm^3 \pm SD$)	Metastatic Incidence*
DU145	5/5	171 ± 96	0/4
DU145-LN1	4/4	718 ± 336	2/4
DU145-LN2	5/5	1904 ± 728	3/4
DU145-LN3	7/7	899 ± 628	5/6
DU145-LN4	4/4	488 ± 312	3/4
DU145-PR3	3/3	313 ± 99	0/3

Cell lines were injected orthotopically into the prostate. Tumors and lymph nodes were removed after 5 weeks.
*Presence of K18-positive metastatic foci in lymph nodes. All available lymph nodes were evaluated.

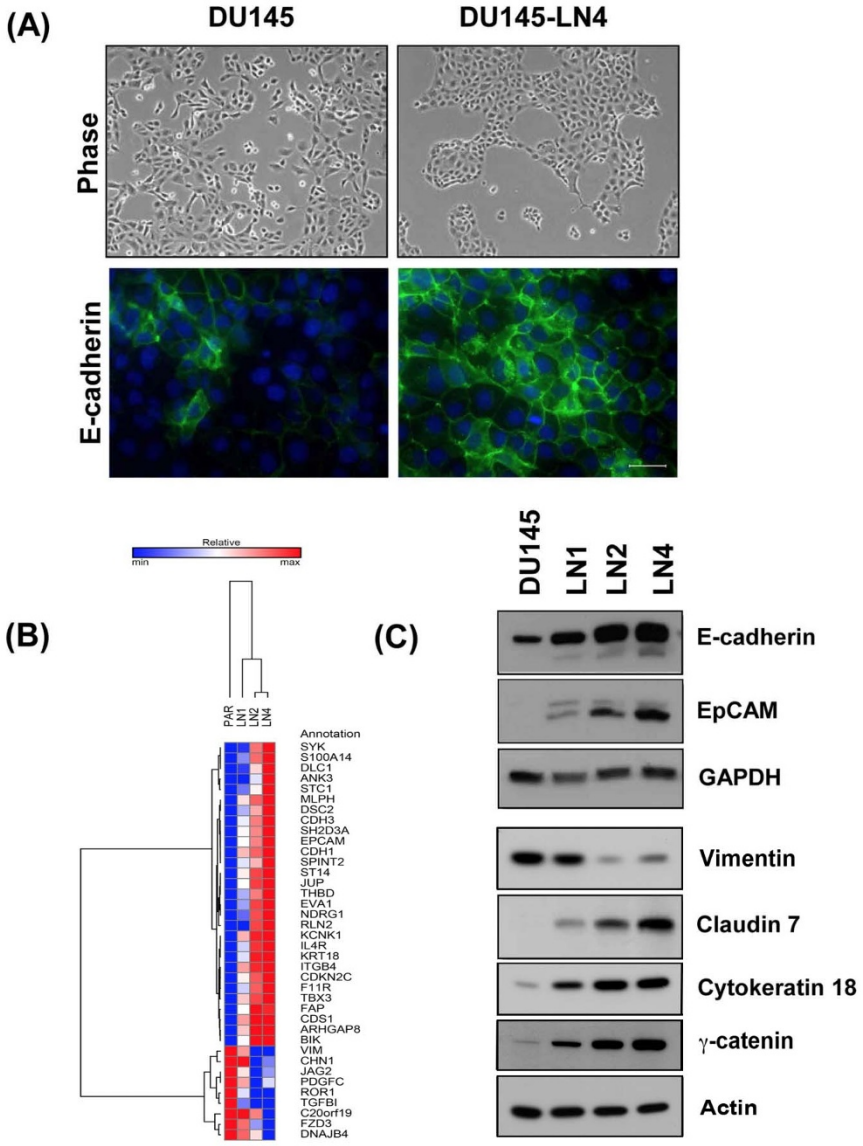

Figure 2 | Metastatic DU145-LN4 cells show mesenchymal to epithelial-like changes. (A) DU145-LN4 cells display more cell–cell clustering as seen by phase microscopy (upper panels), and increased E-cadherin immunostaining (lower panels), scale bar = 50 μm. (B) Microarray analysis shows increased expression of epithelial markers and decreased mesenchymal markers. Heat map diagram shows unsupervised two-way hierarchical clustering of genes and cell lines. Color scale shows relative expression level; red is maximum, blue represents minimum expression level. (C) Western blot confirmed a progressive increase in expression of epithelial markers, and decrease in the mesenchymal marker vimentin, following rounds of metastatic selection from DU145 to DU145-LN4. One membrane was probed for E-cadherin, EpCAM, and GAPDH. Another was probed for vimentin, claudin 7, cytokeratin 18, γ-catenin, and actin. Images were cropped to save space; original images are shown in Supplemental Figure 5.

selection increased the incidence of tumor-cell positive lymph nodes from 0% in mice bearing parental DU145 tumors, to 75% in mice bearing DU145-LN4 tumors (Table 1). We were also able to observe large metastases after H&E staining of the lymph nodes of DU145-LN4-injected mice (Figure 1C). It is important to note that lymph nodes from mice bearing DU145 tumors did not have metastases or obvious K18+ foci, although they did have single K18+ cells at 5 weeks. It is possible that these single K18+ cells would have grown into larger metastases at later time points.

Metastatic DU145-LN4 cells display a more epithelial-like phenotype. The DU145-LN4 metastatic cell line displayed an altered phenotype, compared to parental DU145 cells, showing increased cell-cell interactions and cell clusters indicating a more "epithelial-like" phenotype (Figure 2A, upper panels). E-cadherin immunostaining showed an increased expression level and illustrated the increased cell-cell interactions in the DU145-LN4 cells (Figure 2A, lower panels). The intermediate cell lines, DU145-LN1, LN2 and LN3 also displayed progressively more epithelial-like characteristics (Supplementary Figure 1B). We investigated the gene expression profile of these cells using an Illumina cDNA expression array. Using BRB Array Tools software, data were transformed and normalized as described in Methods. To identify differentially expressed genes, we applied analysis of variance tools typically used for time-course analysis. We selected for linear (positive or negative) gene expression changes, to correspond with the repeated rounds of *in vivo* cycles of lymph node metastasis in our model. We found that many of the genes associated with an epithelial phenotype were dramatically increased. Selection of EMT-related genes[29] showed a pattern of gene expression changes indicating a progressive mesenchymal to epithelial transition (MET) in our model. Expression of the epithelial genes, E-cadherin (CDH1), epithelial cell adhesion molecule (EPCAM), cytokeratin 18 (KRT18), and γ-catenin, also known as junctional plakoglobin (JUP) were significantly increased, and many mesenchymal genes showed decreased expression, including vimentin (VIM) and transforming growth factor β-1(TGFB1) (Figure 2B and 2C). Western blot analysis confirmed these changes at the protein level, with increased expression of E-cadherin, EpCAM, cytokeratin 18, γ-catenin and claudin 7, and decreased vimentin expression (Figure 2C). Our cellular model displays discrete and progressive steps in the process of MET, which correlates with prostate cancer progression.

As a parallel to our *in vivo* metastasis selection model, we also performed repeated rounds of orthotopic prostate injection, establishing tumor cell lines from the prostate (Figure 3A), as described in Methods. This scheme created the *in vivo* prostate-cycled DU145 sublines; DU145-PR1, DU145-PR2 and DU145-PR3. In contrast to the DU145-LN model, repeated *in vivo* cycling through the prostate alone produced no significant change in the metastatic potential of the cells when reinjected *in vivo*. This was assessed by cytokeratin 18 staining of excised lymph nodes as described in Methods. No mice

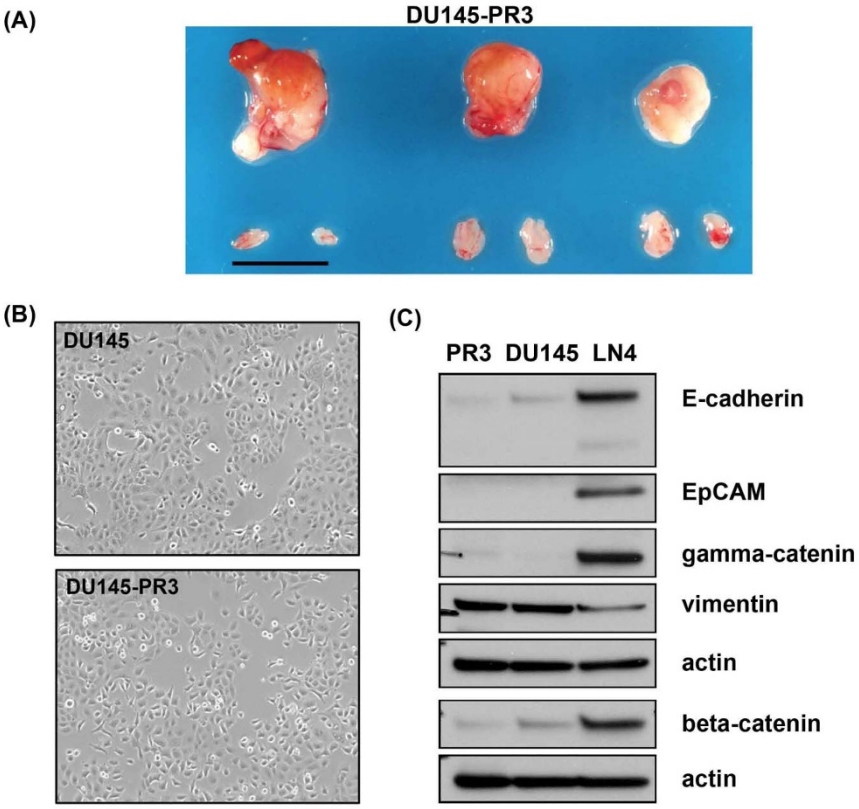

Figure 3 | *In vivo* prostate-cycled DU145 cells do not display the phenotypic and expression changes observed in the metastatic DU145-LN cell lines. DU145 cells were injected into the mouse prostate, the prostate excised and grown in culture to create DU145-PR1. This process was repeated to create DU145-PR2 and DU145-PR3. (A) Photography of DU145-PR3 gross specimens (tumors and sentinel lymph nodes) after 5 weeks following cell line injection orthotopically into the prostate. Scale bar = 1 cm (B) Phase contrast microscopy shows similar cell phenotype of DU145 parental and DU145-PR3 cells in culture. (C) Western blot analysis of DU145-PR3 and parental DU145 cell lysates indicate that expression of E-cadherin, EpCAM, γ-catenin, vimentin and β-catenin were not changed by *in vivo* cycling through the prostate, in contrast to the expression changes observed in DU145-LN4 cells. Equal loading shown by actin immunoblots. The same membrane was stripped and reprobed for E-cadherin, EpCAM, γ-catenin, vimentin, and actin. A separate blot was probed for β-catenin and actin. Images were cropped to save space; original images are shown in Supplemental Figure 5. Handwritten pen marks denote molecular weight markers.

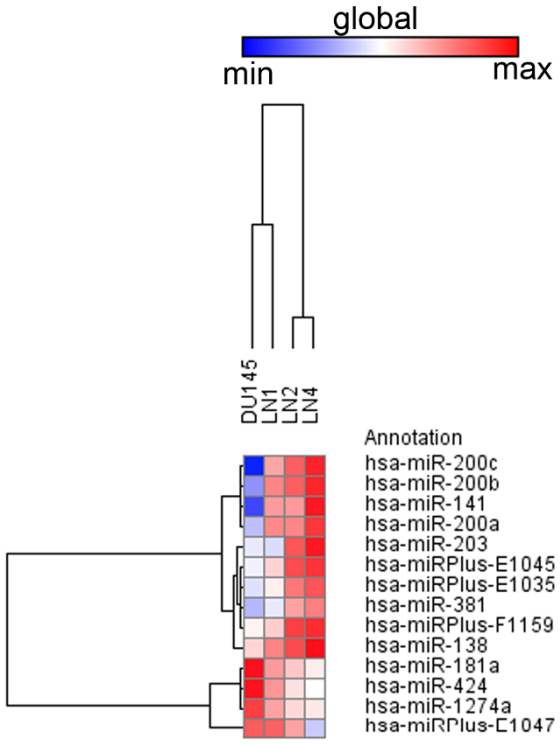

Figure 4 | Heat map profile of miRNA expression in the DU145-LN cell line model. RNA collected from DU145, DU145-LN1, DU145-LN2 and DU145-LN4 was analyzed using a miRCURY LNA array (Exiqon). Hierarchical clustering and heat map representation of miRNAs and cell lines. Global color scale shows maximum (red) and minimum (blue) miRNA expression level.

bearing DU145-PR3 tumors were positive for metastatic foci (Table 1). In contrast to the MET-like changes observed in the metastatic DU145-LN model, no effect was observed in cell morphology (Figure 3B), and no significant change in expression of E-cadherin, EpCAM, β-catenin, γ-catenin or vimentin was observed in DU145-PR3 by Western blot (Figure 3C). This suggests that the microenvironment at the secondary site has a role in either selecting or differentiating tumor cells that arrive at that site.

Cell plasticity is mediated by increased expression of miR-200c and miR-141 in DU145 cells. The MET-like program in these cells suggested a mechanism of coordinated gene expression changes. We examined the miRNA profile in these cells using miRNA gene chips and discovered that several miRNAs showed a pattern of progressively increased or decreased expression across the metastatic DU145 cell line model. The most significantly increased miRNAs in the microarray were those of the miRNA-200 family (miR200a, miR-200b, miR200c and miR-141). The miR-200 family also includes miR-429, which also showed some increased expression in the DU145-LN cell microarray, but did not reach the threshold filter for further analysis. The most significantly decreased miRNA was miR-424 (Figure 4). MiR-200c was the most changed miRNA in the DU145-LN4 microarray data, with 5.5 fold increase in expression relative to parental DU145, miR-141 was the second most changed (4.6 fold), followed by miR-200b (3.2 fold) and miR-200a (2.6 fold).

MiR-200 family expression was investigated using real time RT-PCR. MiR-200a, miR-200b, miR-200c and miR-141 were amplified from three independent RNA collections of the parental DU145, DU145-LN2 and DU145-LN4 cells. Data were normalized to the small housekeeping RNA, SNORD38B. Figure 5A demonstrates that miR-200a, miR-200b, miR-200c and miR-141 expression were progressively increased in DU145-LN2 and DU145-LN4 cells, compared to DU145. MiR-200c and miR-141 showed a greater fold increase in DU145-LN4 relative to DU145 (>7X), compared to miR-200a or miR-200b (approximately 3X). These expression patterns correlated with the miR-200 family microarray data.

We then investigated whether miR-200 inhibition could reverse the epithelial phenotype in DU145-LN4 cells. Cells were transfected with antimiRs to miR-200a, miR-200b, miR-200c and miR-141. MiR-200c and miR-141 are clustered on chromosome 12, separate from the chromosome 1 cluster containing miR-200a, miR-200b and miR-429[30,31]. Clusters are often co-regulated and in our model miR-200c and miR-141 levels were more highly upregulated in DU145-LN4 cells compared to miRs-200a, and -200b. Consequently, antimiRs were also combined in these cluster pairs in addition to combining all four antimiRs. Control cells were transfected with non-specific antimiR controls at matched concentrations between 100–400 nM (day 0). AntimiR-transfected DU145-LN4 cells were monitored by phase microscopy, fixed for immunocytochemistry and whole cell lysates collected at day 3 and day 7. Cells were subjected to a second antimiR transfection on day 7, with samples subsequently collected at day 14. Repeated transfections have been shown to more effectively induce EMT in previous studies[30,32]. We found that antimiR inhibition of the miR-200c and miR-141 cluster resulted in a more mesenchymal phenotype, with reduced cell-cell clustering and cell-cell interactions, as observed by phase microscopy and immunocytochemistry for E-cadherin expression at day 14 (Figure 5B and Supplementary Figure 2). AntimiRs targeting miR-200c or miR-141 were capable of inducing morphologic EMT-like changes to a similar extent when used individually or combined (Figure 5B and Supplementary Figure 2). At the protein level, antimiRs to miR-200c and miR-141 reduced E-cadherin and EpCAM expression by Western blot analysis. MiR-200c treatment caused the most significant induction of vimentin expression (alone or in combination with other miR-200 family members) (Figure 5C). Many of the expression changes in EMT markers were more pronounced after repeated transfection and extended treatment to 14 days. For example, by 14 days, antimiR-141 increased vimentin levels and antimiR to miR-200a inhibited E-cadherin and EpCAM protein expression (Figure 5D). AntimiR to miR-200b showed no significant effect on morphology, E-cadherin immunocytochemical staining or protein marker expression in DU145-LN4 cells. The seed sequences for functional targets are more similar between miR-200a and miR-141, than for miR-200c, miR-200b and miR-429. This suggests that epithelial-mesenchymal plasticity is activated via different mechanisms or potentially through shared targets between the two functional clusters[30,31]. As expected, treatment of DU145-LN4 cells with antimiR-200c and antimiR-141 caused upregulation of the transcription factors, ZEB1 and ZEB2, known mediators of EMT[30–34], paired with reduced E-cadherin (CDH1) expression at the RNA level (Figure 5E).

MET is mediated via loss of miR-424 in DU145-LN4. We discovered a strong inverse correlation of miR-424 expression with the epithelial phenotype in DU145 cells. MiR-424 was the most significantly downregulated miRNA in our microarray analysis (Figure 4), and the level progressively decreased in the DU145-LN cell series as the cells became more epithelial. In microarray data DU145-LN1 showed 1.6 fold, DU145-LN2, 2.1 fold, and DU145-LN4 2.4 fold down-regulation of miR-424 expression, relative to parental DU145 cells (Figure 4). We confirmed this change using real time RT-PCR for miR-424 using RNA prepared from three individual cell cultures. Expression was normalized to the small housekeeping RNA, SNORD38B (Figure 6A). In real time RT-PCR, DU145-LN1 showed only 66% miR-424 expression, LN2 55%, LN3 26% and LN4 25% miR-424 expression, relative to parental DU145 cells (100%).

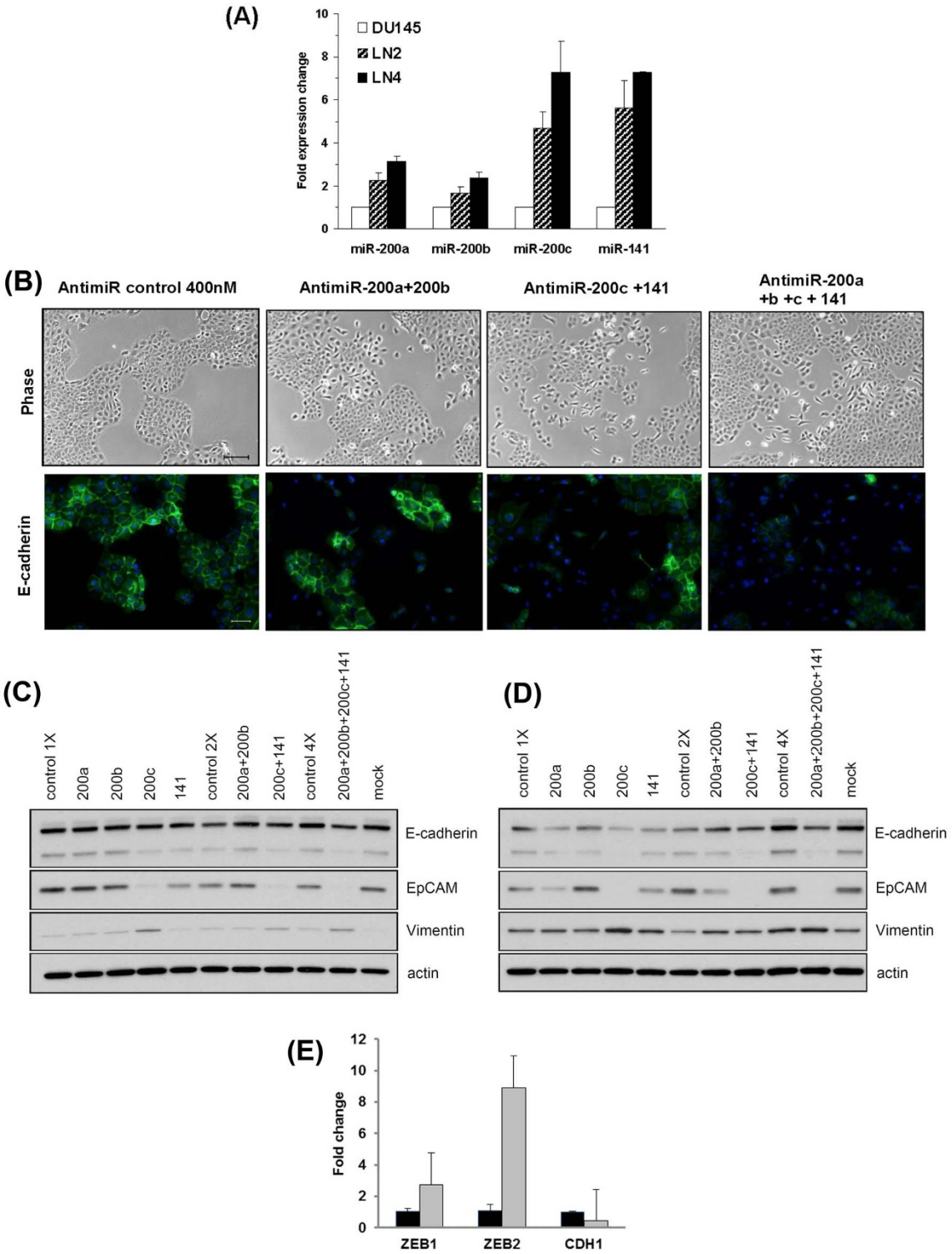

Figure 5 | The miR-200 family regulates EMT in metastatic DU145-LN4 cells. (A) Real time RT-PCR confirmed increased expression of the miR-200 family members; miR-200a, b, c and miR-141 in DU145-LN2 and DU145-LN4 cells, relative to DU145 cells. Mean +/− SEM of triplicates. (B) Treatment of DU145-LN4 cells with a combination of antimiRs to the miR-200a + miR-200b (left center panel) or miR-200c + miR-141 (right center panel) reduced cell clustering and cell-cell interactions, as observed by phase-contrast microscopy (upper panels, scale bar = 100 μm), and E-cadherin immunostaining (lower panels, scale bar = 25 μm) at 14 days. Cells were transfected at day 0 and day 7. (C) Western blot at 7 days (following day 0 transfection) and (D) 14 days (following day 0 and day 7 transfection) showed reduced expression of E-cadherin and EpCAM, and increased vimentin expression following treatment of DU145-LN4 cells with antimiRs 200c + 141. To account for increased antimiR concentration when treated in combination, controls were treated with 200 nM (2X) and 400 nM (4X) non-specific antimiR. Actin shown as protein loading control. The same membrane was stripped and reprobed for each subsequent marker in C or D. Images were cropped to save space; original images are shown in Supplemental Figure 5. (E) Real time RT-PCR amplification of ZEB1, ZEB2 and CDH1 in DU145LN4 cells treated with antimiR-200c + 141 (grey bars), relative to antimiR control (black bars). Data normalized to GAPDH, mean +/− SD.

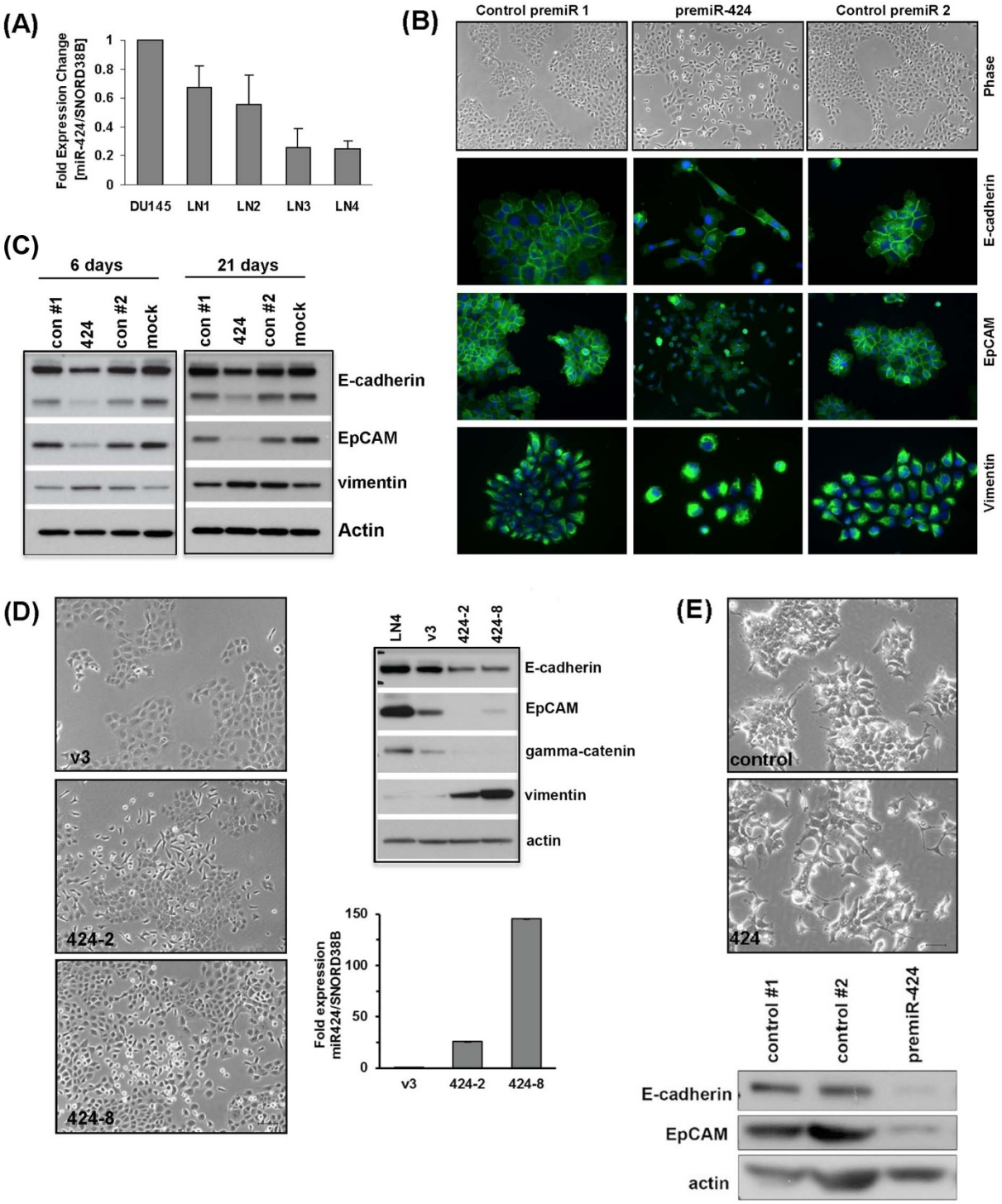

Figure 6 | MiRNA-424 regulates the epithelial phenotype. (A) Progressive downregulation of miR-424 expression in the DU145-LN cell series was measured by real time RT- PCR. (B) DU145-LN4 cells were transfected with two different control premiRs (left and right panels) or premiR-424 (center panel). PremiR-424 induced EMT-like changes, as observed by reduced cell-cell interactions in phase-contrast microscopy, and decreased E-cadherin and EpCAM levels in immunostaining. (C) Western blot analysis of DU145-LN4 cells treated with premiR controls, premiR-424 or mock transfected, collected at 6 and 21 days shows premiR-424 inhibited E-cadherin and EpCAM expression and increased vimentin levels. Actin shown as loading control. (D) Stable overexpression of miR-424 in DU145-LN4 cells resulted in loss of cell-cell contacts as shown by phase contrast microscopy (scale bar 100 μm). DU145-LN4 vector control (v3), and two miR-424-overexpressing DU145-LN4 clones (424-2 and 424-8) shown. Upper right panel shows reduced E-Cadherin, EpCAM and γ-catenin and increased vimentin levels by Western blot. Bar chart of real time PCR data confirmed upregulation of miR-424 level in stable cell lines after normalizing to housekeeping small RNA, SNORD38B. (E) Transient transfection of premiR-424 in epithelial MCF-7 breast cancer cells resulted in increased cell scattering, relative to two individual control premiRNAs, as shown by phase contrast microscopy (scale bar 50 μm). Western blot showed decreased E-Cadherin and EpCAM expression in premiR-424-treated cells. β-actin shown as loading control. Each membrane was stripped and reprobed for each subsequent marker in (C), (D), and (E). Images were cropped to save space; original images are shown in Supplemental Figure 5.

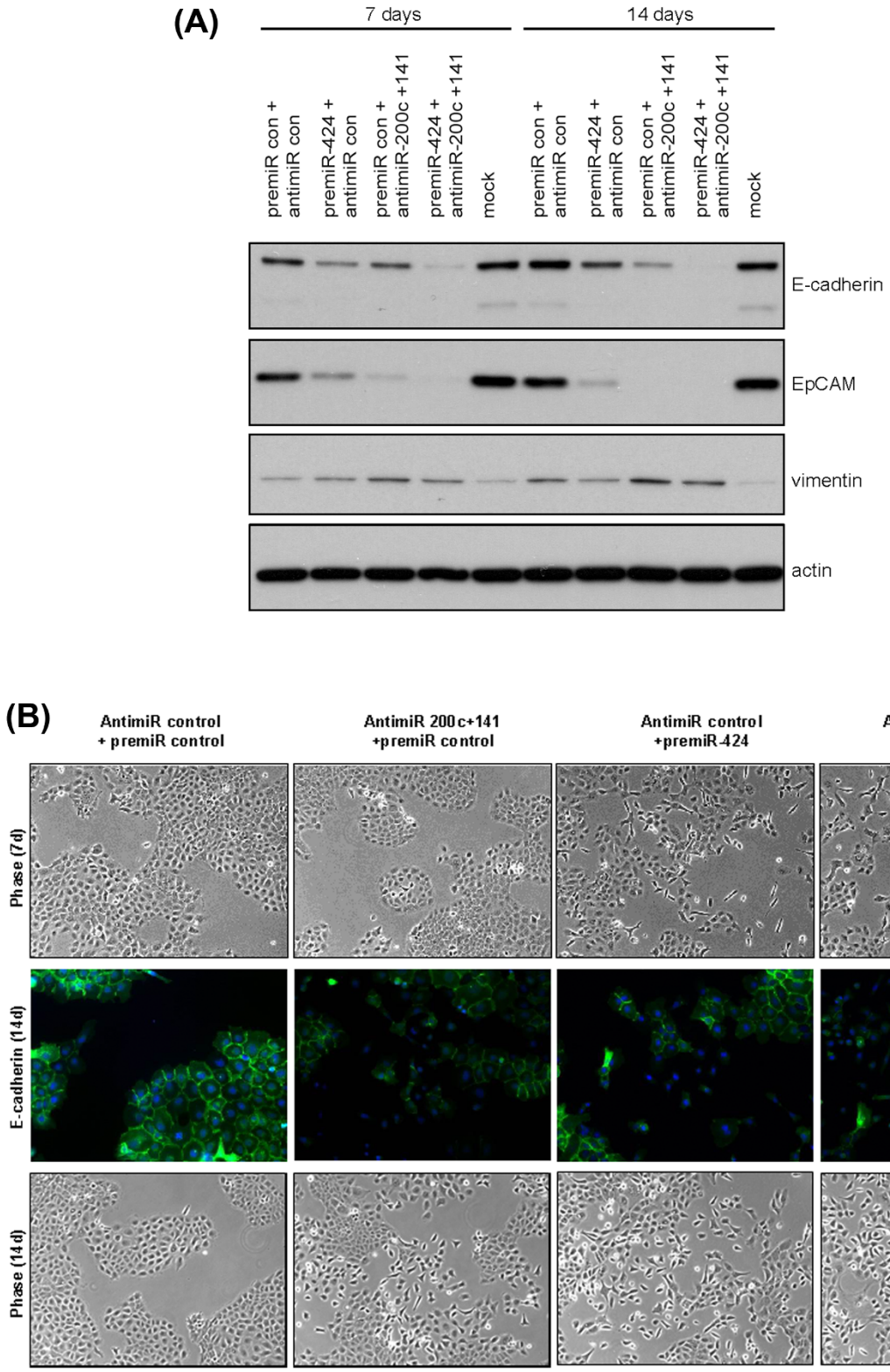

Figure 7 | miR-424 and miR-200c/141 act independently and additively to affect cell plasticity. DU145-LN4 cells were treated with control pre-miR combined with control antimiR, premiR-424 combined with antimiR control, antimiR-200c/141 combined with premiR control, or antimiR-200c/141 combined with premiR-424. (A) Whole cell lysates were collected at 7 and 14 days. Immunoblots showed reduced E-cadherin and EpCAM expression, and increased vimentin levels in premiR-424 or antimiR-200c/141 treated cells. Combining these treatments produced additive inhibition of epithelial markers. The same membrane was stripped and reprobed for each subsequent marker. Images were cropped to save space; original images are shown in Supplemental Figure 5. (B) In parallel with cell lysate collection, treated cells were examined using phase contrast microscopy and E-cadherin immunocytochemistry. Cell scattering was more distinct after premiR-424 treatment at 7 days, compared to antimiR-141/200c. At 14 days we observed additive effects of miR-424 expression and miR-141/200c inhibition, with greater cell scatter and loss of E-cadherin staining.

To determine whether loss of miR-424 expression was involved in the phenotypic MET observed in the DU145 metastasis model, we transfected DU145-LN4 with premiR-424. MiR-424 precursor overexpression induced cell scattering, as observed by phase contrast microscopy and immunocytochemistry (Figure 6B), inhibited expression of the epithelial markers E-cadherin and EpCAM, and increased expression of the mesenchymal marker, vimentin, as seen by Western blot analysis (Figure 6C). MiR-424 overexpression induced similar effects on these EMT markers after a single transfection and protein collection at 6 days, as was seen with second (d7) and third (d14) re-transfections, with lysate collection at d21, respectively (Figure 6C).

MiR-424 was then stably overexpressed in DU145-LN4 cells using a precursor miRNA expression construct (pEZX-miR-424). Stable clones were selected using puromycin, monitored by fluorescence microscopy for GFP, and real time RT-PCR was used to confirm miR-424 overexpression. MiR-424-overexpressing cells showed EMT-like changes in phenotype, with increased cell scattering, loss of E-cadherin expression and gain of vimentin expression (Figure 6D). We observed the same phenotype and expression changes in DU145-LN4 cells when miR-424 was stably overexpressed using an alternative construct, pCMV-miR-424 (Supplementary Figure 3B). Similarly, EpCAM levels decreased and vimentin increased when miR-424 was overexpressed in DU145-LN2 cells (Supplementary Figure 3C–D). To determine whether miR-424 inhibition could induce a reciprocal MET, we transfected antimiR-424 into parental DU145 cells. Inhibition of miR-424 expression increased cell-cell contacts, induced expression of E-cadherin and decreased expression of vimentin, relative to controls (Supplementary Figure 4A–B). Finally, in addition to effects in the DU145 prostate cancer model, transfection of precursor miR-424 induced similar EMT-like changes in other epithelial cell types, including MCF-7 breast cancer cells (Figure 6E).

Additive effects of miR200c/141 cluster inhibition and miR-424 overexpression on cell plasticity. Our data establish a new role for miR-424 in tumor cell plasticity. The miR-200 family has been established as master regulators of EMT[30–32]. However, even against the background of high miR-200 expression, overexpression of miR-424 was capable of inducing EMT.

We sought to determine whether manipulation of the miR-424 and miR-200 pathways could act synergistically to regulate tumor cell EMT. In our model, the epithelial phenotype was represented by high miR-200 and low miR-424 levels. We transfected epithelial DU145-LN4 cells with anti-miR200c/141 and premiR-424, alone or in combination. By Western blot analysis, both miR-424 overexpression and miR-200 inhibition reduced E-cadherin and EpCAM expression and increased vimentin levels, indicating an EMT (Figure 7A). Inhibition of miR-200c and miR-141 had a more dramatic effect on EpCAM and vimentin level, compared to premiR-424 expression. These markers are known to be targets of the miR-200 family; EpCAM has been reported to be a target of miR-200c[35], while vimentin is induced by ZEB[36]. The EMT marker expression changes were supported by phase microscopy and immunocytochemical staining for E-cadherin (Figure 7B), which indicated that at 7 days cell scattering was induced more effectively by miR-424 overexpression, compared to miR-200 inhibition. By combining miR-200c/141 inhibition and miR-424 overexpression, a greater reduction in epithelial marker expression was observed in DU145-LN4 cells after both 7 and 14 days, compared to either treatment alone (Figure 7A and B). However, vimentin was more effectively induced by miR-200c/141 inhibition alone, compared to miR-200c/141 inhibition combined with miR-424 overexpression. Our data suggest that miR-200c/141 and miR-424 influence cell plasticity through additive, rather than synergistic effects.

Discussion

We have created a new spontaneous model of prostate cancer metastasis, and show that a progressive mesenchymal to epithelial transition (MET) occurred as the cells became more metastatic. The role of phenotypic plasticity along an epithelial to mesenchymal axis in cancer progression and metastasis has been widely studied and debated in recent years[3–5,7]. Compelling evidence is now mounting for the importance of an epithelioid phenotype for effective colonization within secondary tumor sites[10–14]. Our data builds upon that evidence and shows *in vivo* selection for MET within a tumor cell population. Our selection criterion was metastasis, without any bias toward phenotype, and we expanded cells that had already successfully reached and survived in the lymph node microenvironment. This indicates spontaneous cell plasticity in response to physical and microenvironment signals. MET occurred in the intrinsically chaotic gene expression of a tumor cell population, and was not driven by ectopic overexpression or inhibition of specific EMT-related transcription factors or miRNAs.

It is quite possible that the EMT/MET status of the cell impacts lymphatic and vascular metastasis differently. In fact, lymphatic capillaries contain open gaps and little to no basement membrane or pericyte coverage, while blood capillaries are surrounded by basement membrane and pericytes[37]. Lymphatic metastasis can use collective cell migration which may better tolerate a more epithelial phenotype, whereas vascular invasion can be aided by the amoeboid motility associated with a more mesenchymal phenotype[38–40]. Circulating miR-141 and 200b correlate with positive lymph node status and metastasis in prostate cancer[41,42]. Importantly, micrometastases must survive and grow at the secondary site to become clinically relevant, and our data supports the importance of an epithelial phenotype in this process.

Due to the background of aberrant gene expression in any tumor cell, the process of tumor EMT is reported to involve many different gene changes dependent on the tumor type. Many genes have been established as epithelial or mesenchymal markers or EMT mediators[2,29,43], but within different systems the expression levels of these are variable and likely driven by different profiles of important regulators such as TGF-β1, transcription factors (including SNAI1, SNAI2, ZEB1, ZEB2 and TWIST1) or miRNAs. E-cadherin loss and vimentin gain are central to the process of EMT, but other key genes in embryonic EMT, e.g. N-cadherin, may be less relevant in some tumor cells. Tumor cells frequently adopt an intermediate phenotype characterized by expression of both epithelial and mesenchymal markers. The nature of this plasticity is being studied intensively by many laboratories.

DU145 human prostate cancer cells have been described as having an "undefined" phenotype because their molecular profile shows expression of both epithelial and mesenchymal expression markers[30]. As such, they provide an excellent starting point for studies on epithelial-mesenchymal plasticity. They show population heterogeneity; epithelial subpopulations have been selected by FACS sorting for E-cadherin[44] and mesenchymal subpopulations selected by cell invasion[45]. Within our DU145-LN model of MET we observe a more comprehensive shift toward epithelial markers (Figure 2), compared to mesenchymal markers. We show that the global shift in EMT/MET related genes is driven by both the miR-200 family and miR-424 in these cells and that they act antagonistically on phenotype. Our data shows multiple changes in epithelial markers upon manipulation of these miRNAs, including E-cadherin, EpCAM, cytokeratin 18, β- and γ-catenins. The miR-200 family is well established as a modulator of EMT. MiR-200 family members bind the transcriptional repressors ZEB1 and ZEB2, resulting in increased E-cadherin levels[30–34], and DU145 express relatively low miR-200b and miR-200c when compared to other cells in the NCI-60 panel of cell lines[12]. In our system miR-200c inhibition caused the most dramatic EMT, among all miR-200 family

members, and upregulation of both ZEB1 and ZEB2 was seen after miR-200c inhibition.

MiR-424 has not previously been shown to mediate tumor plasticity. In our model miR-424 expression could induce epithelial to mesenchymal phenotype changes as effectively as miR-200c. In fact, we consistently observed more dramatic changes in morphology and EMT-related marker expression at an earlier timepoint with miR-424 overexpression, compared to miR-200c inhibition. The additive effects on EMT from combining miR-424 overexpression with miR-200 inhibition suggest these miRNAs are acting on epithelial to mesenchymal plasticity via complementary mechanisms. Certainly, there are no predicted seed sequences for miR-424 in the 3'UTRs of either ZEB1 or ZEB2.

Relatively little is known about the effects of miR-424. In cancer studies, low miR-424 correlates with lymph node metastasis and poor patient outcomes in cervical cancer[46]. In this system the tumor suppressive effects of miR-424 are mediated via protein checkpoint kinase 1 (CHEK1), which did not significantly change in our DU145 model. Another recent report showed inhibition of osteosarcoma cell migration and invasion by miR-424 expression[47]. In non-tumor tissue, miR-424 has been implicated in maintaining the physiology of vasculature[48–51], and blood cell differentiation[52].

MiR-424 is a member of the miR-16 family which includes miRNA-15/16/195/424/497. These miRNAs share a 'seed region' in the 5'UTR which may result in some overlapping miRNA targets[53]. MiR-15a and miR-16 decrease in advanced prostate cancers, with knockdown promoting tumorigenesis[54], and miR-16 delivery reduced growth of prostate tumors in bone[55]. These effects were mediated via cell cycle-related genes BCL2, CCND1, WNT3A[54]. Indeed, in our model, CCND1 mRNA increased with metastatic potential, but DU145-LN4 cells did not show increased proliferation rates, compared to DU145 (J.Banyard, unpublished data). However, it is possible that other overlapping miRNA-16 family targets are involved in the increased tumorigenesis and metastasis that we observe in the DU145-LN metastasis model.

We identified a number of potential miR-424 targets in our system, using MIR@NT@N network analysis[56], which combined miRNA and gene expression data from the DU145-LN model, together with analysis of gene expression data from PremiR-424 overexpression in DU145-LN4 cells. While we validated most of these as targets of miR-424 (e.g. DSC2, F11R, MYB and VAMP8), siRNA knockdown (individually or in combination) was unable to affect cellular plasticity and recapitulate the effects of miR-424 expression in DU145-LN4 cells (J. Banyard, unpublished results). Thus, the mechanism through which miR-424 induces cell plasticity remains under investigation. Our data has identified miR-424 as a novel pivotal actor which is necessary and sufficient to induce EMT and is a new counterbalance of the miR-200 family. Deciphering the different miRNA-424 target networks may be useful for tumor metastasis.

Together, our results provide support for the emerging hypothesis that acquisition of an epithelial phenotype promotes expansion of metastatic colonies. We further provide a novel model that allows interrogation of this process in prostate cancer metastasis. Finally, we implicate miR-424 as a novel regulator of tumor cell plasticity.

Methods

Cell culture and transfection. DU145 human prostate cancer cells were maintained in high glucose DMEM with 10% fetal bovine serum (FBS), 1% glutamine, penicillin and streptomycin (GPS), and 1% sodium pyruvate (Invitrogen, Carlsbad, CA). MCF-7 cells were grown in Eagle's Minimum Essential Medium with 10% FBS, 1% GPS and 0.01 mg/ml human recombinant insulin (Sigma-Aldrich, St. Louis, MO). Cell lines were obtained from ATCC (Manassas, VA).

For transfection, 6×10^5 DU145-LN4 or 2×10^5 DU145 cells were seeded in 6 well plates in serum-containing media. Cells were transfected while in suspension using 25 nM Ambion Pre-miR miRNA precursor (Life Technologies) diluted in OptiMEM media (Invitrogen), and complexed using siLentFect transfection reagent (Biorad, Hercules, CA). Cells were allowed to attach overnight and media replaced the next day. For repeated and extended miRNA treatments, cells were passaged as needed and trypsinized and transfected in suspension at specific time points. Cells were transfected at d0, d7 and d14. Whole cell lysates were collected from d0 transfected cells at d3, d6 and d7, collected from d0 + d7 transfected cells at d14, and d0 + d7 + d14 transfected cells at d21. Pre-miR miRNAs included negative controls #1 and #2 and Pre-miR-424. Control cells were mock transfected in parallel. Loss of function studies were performed by transfection of the miRIDIAN microRNA hairpin inhibitors (Dharmacon/Thermo Scientific), anti-hsa-miR-424, anti-hsa-miR-200a, anti-hsa-miR-200b, anti-hsa-miR-200c and anti-hsa-miR-141 or antimiR control at 100 nM, under the same experimental conditions.

Stable DU145-LN4 and DU145-LN2 cells expressing miR-424 were established by infection with pEZX-MR03 lentiviral vector containing the miRNA precursor clone of hsa-miR-424 (pEZX-miR-424) or scrambled miRNA control clone (GeneCopoeia, Rockville, MD). Expressing clones were selected with puromycin. Additional stable miR-424 overexpressing DU145-LN4 cells were created by FuGENE 6 (Promega, Madison, WI) transfection with pCMV-MIR424 plasmid (Origene Technologies, Rockville, MD). Vector controls were transfected with empty pCMV vector, and stable cells were selected using neomycin.

Phase contrast and fluorescent microscopy images were captured using a Nikon Eclipse TE200 microscope with an RT SPOT camera and SPOT Advanced v4.0.9. software (Diagnostic Instruments, Inc., Sterling Heights, MI).

Western blot analysis. Whole cell lysates were collected in modified RIPA buffer with EGTA and EDTA (Boston Bioproducts, Ashland, MA) with protease inhibitor cocktail (P8340, Sigma-Aldrich). Protein concentration was measured using a BCA protein assay kit (Pierce/Thermo Scientific). 20 μg or 50 μg reduced protein in Laemmli sample buffer was resolved using SDS-PAGE and transferred to Immobilon-P 0.45 μm PVDF membrane (EMD Millipore, Billerica, MA). Membranes were blocked with 5% non-fat dry milk in PBS, incubated with primary antibody, followed by the appropriate secondary IgG antibody; anti-mouse, rabbit or goat-HRP (GE Healthcare). Membranes were washed thoroughly between steps using PBS containing 0.05% Tween, and developed using ECL Plus Western blotting detection kit (GE Healthcare). Primary antibodies used: E-cadherin and β-catenin (BD Biosciences), EpCAM (C-10) and claudin-7 (Santa Cruz Biotechnology, Dallas, TX), vimentin (V9) (Dako, Carpinteria, CA), GAPDH (6C5) (Abcam), β-actin (Sigma), γ-catenin (Cell Signaling Technology), and cytokeratin-18 (Epitomics, Burlingame, CA). Blots were stripped using ReBlot Plus Strong Antibody stripping solution (EMD Millipore) before reprobing.

RNA and miRNA purification and expression analysis. Cells were washed with ice cold PBS and RNA or miRNA purified. RNA was purified using RNeasy mini RNA purification kit (Qiagen). RNA samples were hybridized to an Illumina Ref. 8 bead chip (Illumina, San Diego, CA) at the IDDRC Cell & Molecular Genetics Core Facility, Genetics Division at Boston Children's Hospital. For analysis of miR-424 targets, RNA was collected following 24 hr treatment of DU145-LN4 cells with Pre-miR controls #1 and #2, Pre-miR-424 (Ambion) and syn-hsa-miR-424 (Qiagen). RNA was hybridized to U133 Plus 2.0 gene chips (Affymetrix, Santa Clara, CA). For miRNA analysis, total RNA containing miRNA was purified using an miRNeasy mini kit (Qiagen). MiRNA labeling, hybridization, scanning and expression profiling was performed using miRCURY LNA microarray service (Exiqon).

PCR. Total RNA for PCR was reverse transcribed using iScript cDNA synthesis kit (BioRad). cDNA from DU145, DU145-LN and B16-F10 cell lines was amplified using mouse and human GAPDH primers with iQ SYBR Green Supermix (Biorad) using a DNA Engine Thermal Cycler (Biorad) machine. DNA was separated on a 2% agarose gel containing ethidium bromide. B16-F10 mouse melanoma cell cDNA was included as a positive control for mouse DNA. Real time PCR was performed using a DNA Engine Opticon 2 machine (MJ Research) and analyzed using Opticon 3.1 software (Biorad Laboratories). cDNA was amplified using primers to mouse GAPDH, human GAPDH, CDH1 and ZEB1 (Real Time Primers, Elkins Park, PA), and ZEB2, FWD 5′CAAGAGGCGCAAACAAGC and REV 5′GGTTGGCAATACCGTCATCC[57].

miRNA was copied using the miRCURY LNA Universal cDNA synthesis kit (Exiqon) followed by PCR using iQ SYBR Green Supermix (Biorad) with miRNA LNA PCR primer sets to hsa-miR-200a, has-miR-200b, hsa-miR-200c, hsa-miR-141, hsa-miR-424 and the reference gene primer sets; U6 snRNA (hsa, mmu, rno) and SNORD38B (hsa) (Exiqon). Each sample was amplified in duplicate or triplicate.

Animal studies and development of metastatic DU145-LN model. Orthotopic prostate injection of 8 week male nu/nu mice with DU145 cells and sublines was performed. All animal experiments were approved by the IACUC committee of Boston Children's Hospital. Briefly, mice were anesthetized and an abdominal incision was made to expose the prostate. 2×10^6 cells were injected into the prostate using 40 μl cells in Hanks Balanced Salt Solution in each of two ventral lobes, delivered using a mini-injector. Tumor growth was monitored by palpation. After 5–12 weeks (5 weeks for direct comparison experiment), mice were sacrificed and necropsied to remove tumors and sentinel paraaortic lymph nodes for culture, or formalin fixation, paraffin embedding and tissue analysis. For culture, tissues were washed with PBS, minced through a 100 μM BD Falcon cell strainer (BD Biosciences), washed twice by centrifugation in PBS, and plated on tissue culture dishes in complete media. After attachment overnight, cells were washed thoroughly with PBS, media replaced and cells grown to create DU145-PR1 (from prostate) or DU145-LN1 (from lymph node). After expansion in culture, *in vivo* orthotopic

prostate injection was repeated for additional rounds of selection. Note: while making the cycled model cell lines, lymph nodes were cultured; but in the direct head-to-head comparison of all lines *in vivo*, lymph nodes were embedded and evaluated for metastases.

Immunocytochemistry and immunohistochemistry. For immunocytochemistry, cells were plated on cover slips, and treated in parallel with cells for Western blot analysis. Cells were fixed with 4% paraformaldehyde in PBS at experimental time points. Cells were blocked with 2% BSA in TBS, permeabilized in TBS containing 0.01% Triton X100, and incubated with E-cadherin primary antibody (BD-Biosciences) and anti-mouse Alexa Fluor-488 (Invitrogen). Nuclei were stained using DAPI and coverslips mounted with Vectashield mounting media (Vector Labs). No significant staining was seen with secondary antibody controls.

For tissue immunohistochemistry, paraffin embedded lymph nodes were rehydrated and stained with hematoxylin and eosin, or cytokeratin-18. Heat induced epitope retrieval was performed with citrate buffer (pH 6). Tissue was blocked using normal serum and incubated with cytokeratin 18 antibody (Epitomics) and biotinylated anti-rabbit (Vector Laboratories, Burlingame, CA) followed by Vectastain Elite (avidin-HRP; Vector), and developed with diaminobenzidine (DAB, Vector). To detect human epithelial cell metastases, sentinel lymph node sections were stained with cytokeratin 18 antibody and counterstained with hematoxylin. Sections were examined by microscopy and cytokeratin 18 positive cells grouped in small foci were scored as metastases. Three different tissue levels from each of two lymph nodes (when available) were examined per mouse.

Statistical analysis. miRNA microarray data was analyzed by miRCURY LNA microarray service (Exiqon). Data was normalized using the non-parametric regression method, LOESS. Unsupervised two-way clustering of miRNAs and samples was performed on log2 (Hy3/Hy5) ratios (with each sample versus the common reference pool) to produce a heat map. Illumina Ref. 8 gene expression data from the DU145-LN metastasis model was processed using average normalization with background subtraction. Normalized data was analyzed using BRB-ArrayTools (Biometrics Research Branch, National Cancer Institute) and analysis of variance across a time course of DU145 < DU145-LN1 < DU145-LN2 < DU145-LN4 groups was performed. Heat map expression data was displayed using Gene-E software developed by Joshua Gould (http://www.broadinstitute.org/cancer/software/GENE-E). Hierarchical clustering using one minus Pearson's correlation was applied to samples and genes/miRNAs. Global or relative map colors were applied using the minimum and maximum values in the data. Network analysis to identify miRNA targets using gene and miRNA expression data was performed using MIR@NT@N[56].

1. Gupta, G. P. & Massague, J. Cancer metastasis: building a framework. *Cell* **127**, 679–695 (2006).
2. Kalluri, R. & Weinberg, R. A. The basics of epithelial-mesenchymal transition. *J Clin Invest* **119**, 1420–1428 (2009).
3. Tarin, D., Thompson, E. W. & Newgreen, D. F. The fallacy of epithelial mesenchymal transition in neoplasia. *Cancer Res* **65**, 5996–6000; discussion 6000-5991; (2005).
4. Thompson, E. W., Newgreen, D. F. & Tarin, D. Carcinoma invasion and metastasis: a role for epithelial-mesenchymal transition? *Cancer Res* **65**, 5991–5995 discussion 5995 (2005).
5. Garber, K. Epithelial-to-mesenchymal transition is important to metastasis, but questions remain. *J Natl Cancer Inst* **100**, 232–233 239 (2008).
6. Ledford, H. Cancer theory faces doubts. *Nature* **472**, 273 (2011).
7. Chui, M. H. Insights into cancer metastasis from a clinicopathologic perspective: Epithelial-Mesenchymal Transition is not a necessary step. *Int J Cancer* **132**, 1487–1495 (2013).
8. Weinberg, R. A. Leaving home early: reexamination of the canonical models of tumor progression. *Cancer Cell* **14**, 283–284 (2008).
9. Brabletz, T. To differentiate or not--routes towards metastasis. *Nat Rev Cancer* **12**, 425–436 (2012).
10. Chaffer, C. L. *et al.* Mesenchymal-to-epithelial transition facilitates bladder cancer metastasis: role of fibroblast growth factor receptor-2. *Cancer Res* **66**, 11271–11278 (2006).
11. Chao, Y. L., Shepard, C. R. & Wells, A. Breast carcinoma cells re-express E-cadherin during mesenchymal to epithelial reverting transition. *Mol Cancer* **9**, 179 (2010).
12. Korpal, M. *et al.* Direct targeting of Sec23a by miR-200s influences cancer cell secretome and promotes metastatic colonization. *Nat Med* **17**, 1101–1108 (2011).
13. Tsai, J. H., Donaher, J. L., Murphy, D. A., Chau, S. & Yang, J. Spatiotemporal regulation of epithelial-mesenchymal transition is essential for squamous cell carcinoma metastasis. *Cancer Cell* **22**, 725–736 (2012).
14. Ocana, O. H. *et al.* Metastatic colonization requires the repression of the epithelial-mesenchymal transition inducer Prrx1. *Cancer Cell* **22**, 709–724 (2012).
15. Tse, J. C. & Kalluri, R. Mechanisms of metastasis: epithelial-to-mesenchymal transition and contribution of tumor microenvironment. *J Cell Biochem* **101**, 816–829 (2007).
16. Zhang, J. & Ma, L. MicroRNA control of epithelial-mesenchymal transition and metastasis. *Cancer Metastasis Rev* **31**, 653–662 (2012).
17. Bullock, M. D., Sayan, A. E., Packham, G. K. & Mirnezami, A. H. MicroRNAs: critical regulators of epithelial to mesenchymal (EMT) and mesenchymal to epithelial transition (MET) in cancer progression. *Biol Cell* **104**, 3–12 (2012).
18. Siegel, R. *et al.* Cancer treatment and survivorship statistics, 2012. *CA Cancer J Clin* **62**, 220–241 (2012).
19. Cheng, L. *et al.* Lymphovascular invasion is an independent prognostic factor in prostatic adenocarcinoma. *J Urol* **174**, 2181–2185 (2005).
20. Karakiewicz, P. I. & Hutterer, G. C. Predictive models and prostate cancer. *Nat Clin Pract Urol* **5**, 82–92 (2008).
21. Sleeman, J. P. & Thiele, W. Tumor metastasis and the lymphatic vasculature. *Int J Cancer* **125**, 2747–2756 (2009).
22. Wilt, T. J. *et al.* Radical prostatectomy versus observation for localized prostate cancer. *N Engl J Med* **367**, 203–213 (2012).
23. Stephenson, R. A. *et al.* Metastatic model for human prostate cancer using orthotopic implantation in nude mice. *J Natl Cancer Inst* **84**, 951–957 (1992).
24. Fidler, I. J. The organ microenvironment and cancer metastasis. *Differentiation* **70**, 498–505 (2002).
25. Hanahan, D. & Weinberg, R. A. Hallmarks of cancer: the next generation. *Cell* **144**, 646–674 (2011).
26. Sottnik, J. L., Zhang, J., Macoska, J. A. & Keller, E. T. The PCa Tumor Microenvironment. *Cancer Microenviron* **4**, 283–297 (2011).
27. Pettaway, C. A. *et al.* Selection of highly metastatic variants of different human prostatic carcinomas using orthotopic implantation in nude mice. *Clin Cancer Res* **2**, 1627–1636 (1996).
28. Stone, K. R., Mickey, D. D., Wunderli, H., Mickey, G. H. & Paulson, D. F. Isolation of a human prostate carcinoma cell line (DU 145). *Int J Cancer* **21**, 274–281 (1978).
29. Taube, J. H. *et al.* Core epithelial-to-mesenchymal transition interactome gene-expression signature is associated with claudin-low and metaplastic breast cancer subtypes. *Proc Natl Acad Sci U S A* **107**, 15449–15454 (2010).
30. Park, S. M., Gaur, A. B., Lengyel, E. & Peter, M. E. The miR-200 family determines the epithelial phenotype of cancer cells by targeting the E-cadherin repressors ZEB1 and ZEB2. *Genes Dev* **22**, 894–907 (2008).
31. Korpal, M., Lee, E. S., Hu, G. & Kang, Y. The miR-200 family inhibits epithelial-mesenchymal transition and cancer cell migration by direct targeting of E-cadherin transcriptional repressors ZEB1 and ZEB2. *J Biol Chem* **283**, 14910–14914 (2008).
32. Gregory, P. A. *et al.* The miR-200 family and miR-205 regulate epithelial to mesenchymal transition by targeting ZEB1 and SIP1. *Nat Cell Biol* **10**, 593–601 (2008).
33. Hurteau, G. J., Carlson, J. A., Spivack, S. D. & Brock, G. J. Overexpression of the microRNA hsa-miR-200c leads to reduced expression of transcription factor 8 and increased expression of E-cadherin. *Cancer Res* **67**, 7972–7976 (2007).
34. Burk, U. *et al.* A reciprocal repression between ZEB1 and members of the miR-200 family promotes EMT and invasion in cancer cells. *EMBO Rep* **9**, 582–589 (2008).
35. Cochrane, D. R., Spoelstra, N. S., Howe, E. N., Nordeen, S. K. & Richer, J. K. MicroRNA-200c mitigates invasiveness and restores sensitivity to microtubule-targeting chemotherapeutic agents. *Mol Cancer Ther* **8**, 1055–1066 (2009).
36. Bindels, S. *et al.* Regulation of vimentin by SIP1 in human epithelial breast tumor cells. *Oncogene* **25**, 4975–4985 (2006).
37. Zwaans, B. M. & Bielenberg, D. R. Potential therapeutic strategies for lymphatic metastasis. *Microvasc Res* **74**, 145–158 (2007).
38. Friedl, P. & Gilmour, D. Collective cell migration in morphogenesis, regeneration and cancer. *Nat Rev Mol Cell Biol* **10**, 445–457 (2009).
39. Giampieri, S. *et al.* Localized and reversible TGFbeta signalling switches breast cancer cells from cohesive to single cell motility. *Nat Cell Biol* **11**, 1287–1296 (2009).
40. Hager, M. H. *et al.* DIAPH3 governs the cellular transition to the amoeboid tumour phenotype. *EMBO Mol Med* **4**, 743–760 (2012).
41. Brase, J. C. *et al.* Circulating miRNAs are correlated with tumor progression in prostate cancer. *Int J Cancer* **128**, 608–616 (2011).
42. Mitchell, P. S. *et al.* Circulating microRNAs as stable blood-based markers for cancer detection. *Proc Natl Acad Sci U S A* **105**, 10513–10518 (2008).
43. Zeisberg, M. & Neilson, E. G. Biomarkers for epithelial-mesenchymal transitions. *J Clin Invest* **119**, 1429–1437 (2009).
44. Putzke, A. P. *et al.* Metastatic progression of prostate cancer and e-cadherin regulation by zeb1 and SRC family kinases. *Am J Pathol* **179**, 400–410 (2011).
45. Chunthapong, J. *et al.* Dual roles of E-cadherin in prostate cancer invasion. *J Cell Biochem* **91**, 649–661 (2004).
46. Xu, J. *et al.* Suppressed miR-424 expression via upregulation of target gene Chk1 contributes to the progression of cervical cancer. *Oncogene* **32**, 976–987 (2012).
47. Long, X. H. *et al.* Tumor suppressive microRNA-424 inhibits osteosarcoma cell migration and invasion via targeting fatty acid synthase. *Exp Ther Med* **5**, 1048–1052 (2013).
48. Ghosh, G. *et al.* Hypoxia-induced microRNA-424 expression in human endothelial cells regulates HIF-alpha isoforms and promotes angiogenesis. *J Clin Invest* **120**, 4141–4154 (2010).
49. Kim, J. *et al.* An endothelial apelin-FGF link mediated by miR-424 and miR-503 is disrupted in pulmonary arterial hypertension. *Nat Med* **19**, 74–82 (2013).
50. Nakashima, T. *et al.* Down-regulation of mir-424 contributes to the abnormal angiogenesis via MEK1 and cyclin E1 in senile hemangioma: its implications to therapy. *PLoS One* **5**, e14334 (2010).

51. Chamorro-Jorganes, A. *et al.* MicroRNA-16 and microRNA-424 regulate cell-autonomous angiogenic functions in endothelial cells via targeting vascular endothelial growth factor receptor-2 and fibroblast growth factor receptor-1. *Arterioscler Thromb Vasc Biol* **31**, 2595–2606 (2011).
52. Rosa, A. *et al.* The interplay between the master transcription factor PU.1 and miR-424 regulates human monocyte/macrophage differentiation. *Proc Natl Acad Sci U S A* **104**, 19849–19854 (2007).
53. Forrest, A. R. *et al.* Induction of microRNAs, mir-155, mir-222, mir-424 and mir-503, promotes monocytic differentiation through combinatorial regulation. *Leukemia* **24**, 460–466 (2010).
54. Bonci, D. *et al.* The miR-15a-miR-16-1 cluster controls prostate cancer by targeting multiple oncogenic activities. *Nat Med* **14**, 1271–1277 (2008).
55. Takeshita, F. *et al.* Systemic delivery of synthetic microRNA-16 inhibits the growth of metastatic prostate tumors via downregulation of multiple cell-cycle genes. *Mol Ther* **18**, 181–187 (2010).
56. Le Bechec, A. *et al.* MIR@NT@N: a framework integrating transcription factors, microRNAs and their targets to identify sub-network motifs in a meta-regulation network model. *BMC Bioinformatics* **12**, 67 (2011).
57. Fassina, A. *et al.* Epithelial-mesenchymal transition in malignant mesothelioma. *Mod Pathol* **25**, 86–99 (2012).

Acknowledgments

Research reported in this publication was supported by grants from the Prostate Cancer Foundation (BRZ), and by the National Institutes of Health under award numbers, NIH R01 CA37393 (BRZ), NIH R21 CA155728 (DRB) and NIH K01 CA118732 (DRB). This content is solely the responsibility of the authors and does not necessarily represent the official views of the National Institutes of Health. We thank Courtney Barrows, Milind Chalishazar and Andrea Henricks for technical assistance, Melissa Anderson for administrative assistance, and Kristin Johnson for graphical preparation of figures. We acknowledge Ricardo Sanchez, HTL (Ricasan Histology Consultants) for tissue sections.

Author contributions

J.B. conceived the experiments, performed all the experiments, analyzed and interpreted data, and wrote the manuscript. I.C. contributed to the experimental design and edited the manuscript, A.M.W. performed experiments in Fig. 2, 5, 6 and 7. G.V. and A.L.B. analyzed and interpreted data and edited the manuscript. D.R.B. conceived the experiments, performed the experiments in Fig. 1, Fig. 3 and Table 1, analyzed and interpreted data, contributed to the experimental design and edited the manuscript. B.R.Z. conceived the experiments and edited the manuscript.

Additional information

Accession Codes: The data discussed in this publication have been deposited in NCBI's Gene Expression Omnibus and are accessible through GEO SuperSeries record number GSE51756.

Supplementary information accompanies this paper at http://www.nature.com/scientificreports

Competing financial interests: The authors declare no competing financial interests.

How to cite this article: Banyard, J. *et al.* Regulation of epithelial plasticity by miR-424 and miR-200 in a new prostate cancer metastasis model. *Sci. Rep.* **3**, 3151; DOI:10.1038/srep03151 (2013).